Journal of Radioanalytical and Nuclear Chemistry (2021) 329:159–169
https://doi.org/10.1007/s10967-021-07757-1

Degradation of pyrazinamide in aqueous solution by electron beam irradiation: kinetics, influence factors and mechanism study

Qi Zou[1] · Zhuhao Huo[1] · Haiyang Shao[1] · Jianzhong Gu[1] · Gang Xu[1,2]

Received: 18 January 2021 / Accepted: 24 April 2021 / Published online: 20 May 2021

Abstract

The degradation of pyrazinamide (PZA) by electron beam irradiation (EBI) was studied. It was found that the degradation of PZA was efficient with the removal rate of 99% for 0.2 mM PZA under 5 kGy, and the degradation kinetics followed pseudo-first-order kinetics. The presence of CO_3^{2-}, HCO_3^-, NO_3^-, and fulvic acid inhibited the degradation of PZA. The addition of H_2O_2 or $K_2S_2O_8$ effectively enhanced the degradation and mineralization of PZA. The scavenger experiments and quantum chemical calculations showed that ·OH was the primary reactive species in the degradation. The identification of intermediates and quantum chemical calculations illustrated the mechanism of degradation.

Keywords Pyrazinamide · Electron beam · Radiolysis · Degradation · Degradation mechanism · Quantum chemistry calculation

Article Highlights

1. The degradation of pyrazinamide in aqueous solution by electron beam irradiation was highly efficient.
2. The addition of H_2O_2 or $K_2S_2O_8$ improved the degradation and mineralization of pyrazinamide.
3. The degradation mechanism of pyrazinamide was studied by the experimental results and quantum chemical calculations.

✉ Haiyang Shao
shy2018@shu.edu.cn

✉ Gang Xu
xugang@shu.edu.cn

Qi Zou
sherlock29@shu.edu.cn

Zhuhao Huo
huozhuhao@163.com

Jianzhong Gu
jzhgu@staff.shu.edu.cn

[1] School of Environmental and Chemical Engineering, Shanghai University, 99 Shangda Road, Shanghai 200444, People's Republic of China

[2] Key Laboratory of Organic Compound Pollution Control Engineering, Ministry of Education, Shanghai 200444, People's Republic of China

Introduction

In recent years, the presence of antibiotics in water has received much attention [1–3]. Conventional wastewater treatments have limited effectiveness in treating most antibiotics in water and lead to the persistence of antibiotics and their metabolites in an aqueous environment [4]. In the past, the concentrations of antibiotics in the various environment samples ranging from ng L^{-1} to μg L^{-1} have been detected worldwide [5]. As a communicable antibiotic, PZA is used to treat tuberculosis. In 2019, there are predictable 10 million people developed tuberculosis [6]. Usually, most people who develop tuberculosis need about six months to be cured with first-line antibiotics [6], so tones of PZA is consumed to treat tuberculosis. It is reported that approximately 30% of PZA is absorbed in the body during the 24 h [7]. PZA is detected in a wastewater treatment plant near a pharmaceutical factory in India [8]. It is reported that the predicted environmental concentration of PZA is 7.5 ug/L in China [9]. Moreover, PZA and its metabolites can induce bacterial resistance at low concentrations [10, 11]. Therefore, it is necessary to achieve the effective removal of PZA in the water treatment.

The advanced oxidation processes (AOPs) based on rapidly generating powerful hydroxyl radicals (·OH) which react non-selectively with most organic compounds, are considered a potential technique to reduce pharmaceuticals,

including antibiotics from water compared to the conventional treatment process [12, 13]. It is reported that TiO_2 shows photocatalytic activity on the degradation of PZA under UV irradiation [14, 15]. However, the efficiency of UV degradation may be reduced in treating surface water due to the absorption of UV energy by suspended solids [16]. Photo-Fenton [17] and electron-Fenton [18] techniques are studied to degrade PZA in the aqueous medium, although the issues about iron sludge and higher current need to be solved. In addition, all the above degradation techniques require a long time.

EBI is particularly suitable for the degradation of persistent organic compounds due to its simplicity and high degradation efficiency [19]. High radiation energy can effectively degrade organic compounds in aqueous, such as pharmaceuticals personal care products [20] (PPCPs), antibiotics [21] and dyes [22]. Besides, EBI is a special AOP due to the simultaneous generation of the reductive species (e_{aq}^-, $H^{\cdot}$) and oxidative species ($^{\cdot}OH$) in water radiolysis (Eq. 1) [23]. Therefore, some organic pollutants in water challenging to be degraded by $^{\cdot}OH$ can be removed through the reductive species generated by water radiolysis [24].

$$H_2O \rightsquigarrow e_{aq}^-(2.6) + H^{\cdot}(0.6) + {}^{\cdot}OH(2.7) + H_2O_2(0.7) + H_2(0.45) + H^+(2.6) \quad (1)$$

The degradations of most organic pollutants include a set of complex reactions [25, 26]. It is hard to comprehend the detailed degradation mechanism of organic compounds only through experiments. Quantum chemistry calculation is a standard method to research the degradation mechanism of organic pollutants [26–29]. It is reported that quantum chemistry calculation is used to successfully explain the degradation mechanism of cyanuric acid [27]. Therefore, to forecast the predominant reaction pathway and understand the degradation mechanism of PZA by EBI, quantum chemistry calculations and experiments analysis are used concurrently.

In this paper, the degradation of PZA in aqueous solution by EBI and the influence of different environmental factors on the degradation were investigated. Moreover, the degradation mechanism was illustrated through degradation products analysis and quantum chemical calculations. The experiments were performed: (1) the effects of PZA initial concentrations, irradiation doses, and water matrices; (2) the effects of anions and organic matter that were possibly present in water, such as Cl^-, CO_3^{2-}, HCO_3^-, NO_3^-, NO_2^-, SO_4^{2-}, and fulvic acid; (3) the effects of combining hydrogen peroxide or potassium persulfate with EBI; (4) the effects of initial solution pH and some scavengers. Finally, the calculations of chemical reaction thermodynamic and chemical reaction kinetic are performed.

Materials and methods

Chemicals

Pyrazinamide ($M_W = 123.11$) and fulvic acid ($M_W = 308.24$) with 98% purity were purchased from J&K Chemical Ltd. (Shanghai, China). Sodium chloride, sodium carbonate, sodium bicarbonate, sodium sulfate, sodium nitrite, and sodium nitrate were analytic grade reagents purchased from Shanghai Aladdin Biochemical Technology Co., Ltd. Tert-butanol, sulfuric acid, sodium hydroxide, potassium persulfate, and hydrogen peroxide were analytic grade reagents purchased from J&K Chemical Ltd. (Shanghai, China). Methanol (HPLC), methanol (HPLC–MS), and formic acid (HPLC–MS) were purchased from ANPEL Laboratory Technologies (Shanghai) Inc. Deionized water (resistance > 18.2 MΩcm) was prepared using the Milli-Q-Plus ultra-pure water system from Millipore (Sartorius 611, Germany).

Irradiation source and methods

The electron accelerator (GJ-2-II) with a beam energy of 1.8 meV and variable current (0–10 mA) was manufactured by Xianfeng electrical plant and belonged to the Institute of Applied Radiation, Shanghai University, China. The PZA solution was packed in 0.1 mm thick polyethylene bags (12 cm × 10 cm) and irradiated at different irradiation doses at room temperature (25 °C). The absorbed dose was determined using a Fricke dosimeter, which showed 176 Gy absorbed dose per 500 Gy irradiation dose. In addition, all sample solutions except for the N_2O-saturated experiments were purged with N_2 before irradiation.

Analytical methods

The analytical instruments in this paper include the ultra-high-performance liquid chromatography (UHPLC), the high-performance liquid chromatography–mass spectrometry (LC–MS), the ion chromatography (IC), and the total organic carbon (TOC) analysis. In this study, all analyzed solutions were filtered through a 0.45 μm polytetrafluoroethylene (PTFE) filter membrane. The detailed analysis is available in the supplementary material.

Computational details

All calculations of solution-phase free energy used the following formula [30]:

$$G_{soln} = G_{gas} + \Delta G_{solv} + RT \ln\left(\frac{RT}{P}\right) \quad (2)$$

where the G_{gas} is the value of the free energy in the gas phase, the ΔG_{solv} is the value of the free energy of solvation, and the $RT \ln\left(\frac{RT}{P}\right)$, the change of energy from the gas phase standard state to the solution phase standard state, is 1.8 kcal mol^{-1}. In this study, G_{gas} is equal to the sum of the high precision single-point energy and the low precision free energy correction, and ΔG_{solv} is equal to the difference between the single-point energy under the SMD [31] solvation model and the gas phase single-point energy.

First, Gaussian 09 program [32] was used to carry out the calculations of geometrical optimizations and vibrational frequency analyses. The calculations were performed at the M06-2x/6-311 g(d,p) level of theory, which was more cost-effective for studying organic compounds [33], with SMD in water as the continuum solvation model and the Grimme's DFT-D3 correction [34, 35] as dispersion corrected method. All stationary points (no imaginary frequency) and transition states (only single imaginary frequency) were identified by vibrational frequency analyses. Secondly, to obtain free energy correction, Shermo 2.0.5 [36] was used to calculate molecular thermodynamic properties under the conditions of 298.15 K and 1 atm. In order to improve the accuracies of the zero-point energy (ZPE) and internal energy (U), the frequency scale factors for calculating ZPE and U were 0.970 and 0.983[37], respectively. Thirdly, the high precision single-point energy calculations were using Orca 4.2 program [38, 39] with the PWPB95-D3(BJ)/def2-QZVPP level of theory on the optimized structures. Fourthly, the calculations of solvation free energy were performed through the difference of the single-point energy between the M05-2x/6-31G(d) level with the SMD model and M05-2x/6-31G(d) on the same optimized structures. It is reported that the M05-2× functional with the 6-31g(d) basic set is more suitable for the SMD model [31]. Finally, the final solution-phase free energy was obtained by Eq. (2).

Moreover, intrinsic reaction coordinate (IRC) calculations verified the correctness of the transient state (TS). The calculation of the Reactions of radicals' combination used the downhill method in IRC. The traditional transition state theory [40] (TST) was used to calculate chemical reaction kinetics k^{TST}:

$$k^{TST} = n\kappa \frac{k_B T}{h} \frac{Q_{TS}}{Q_R} e^{-\frac{\Delta G^0}{RT}} \quad (3)$$

where n is the reaction path degeneracy, κ is the transmission coefficient calculated by the Skodje-Truhlar method [41], k_B is Boltzmann constant, T is the thermodynamic temperature (K), h is Planck constant, Q_{TS} and Q_R are the partition function of transition state and reactants respectively, ΔG^0 is the free energy difference between the reactants and the transition state, and R is gas constant. In addition, to avoid confusion, k represents the reaction rate constant obtained from the reference, and k^{TST} represents the reaction rate constant by calculated.

Results and discussion

Degradation kinetics

Figure 1 shows the distinction of PZA removals following different irradiation doses and initial concentrations. The efficiency of PZA removals are positively correlated with irradiation doses at all initial concentrations and negatively correlated with initial concentrations at the same irradiation dose. It can be attributed to the relative concentrations of PZA and reactive species. At higher doses and lower initial concentrations, the higher relative concentration of PZA increases the removal efficiency.

Radiation-chemical yield (G-value) is the number of molecules produced or consumed with the absorption of 100 eV of radiation energy. The calculation formula is as follows:

$$G = \frac{(C_0 - C)\,NA}{6.24 \times 10^{19}\,D}$$

where C_0 and C are the PZA concentration (M) the initial concentration and at the absorbed dose of D (kGy), respectively; NA is Avogadro constant; 6.24×10^{19} is the conversion factor of kGy to 100 eV L^{-1}.

The G-value are showed in Table S1. G-value is positively correlated with the initial PZA concentration at the same irradiation dose and negatively correlated with the irradiation dose at the same initial PZA concentration. The reason for the decrease in G-value may be the competition of by-products with PZA molecules for reactive radicals.

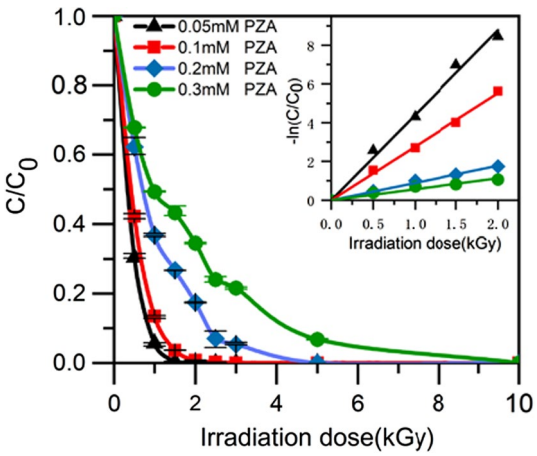

Fig. 1 Degradation of PZA at different initial concentrations and irradiation doses

The PZA degradation kinetics accords with the pseudo-first order kinetics (Eq. 4).

$$\ln \frac{C}{C_0} = -k_d D \tag{4}$$

where k_d is the dose constant (kGy^{-1}), C and C_0 are the PZA concentration (mM) at the irradiation dose of D (kGy) and the initial concentration, respectively.

The reaction dose constants are 4.39 (±0.06), 2.77 (±0.03), 0.89 (±0.03) and 0.57 (±0.02) kGy^{-1} with initial concentrations of 0.05, 0.1, 0.2 and 0.3 mM respectively, suggesting that the reaction dose constant decrease with the increased of the initial PZA concentration. The reason for this is that the increased intermediates of PZA degradation compete with PZA molecules for the reactive species generated by water radiolysis, and the amount of reactive species is proportional to the irradiation dose.

Effects of solution pH and water components

Figure 2a indicates the effects of solution pH on PZA degradations. The PZA degradation is decreased in alkaline condition comparing with neutral condition, while negligible effect in acidic condition. The k_d values are 0.93 (±0.02), 0.89 (±0.03), 0.31 (±0.03) kGy^{-1} at pH = 4, 7.5, and 11, respectively. Solution pH is related to the G values of reactive species generated by water radiolysis, which decide the degradation efficiency of PZA. It is reported that the sum ($Ge_{aq}^- + G_{H\cdot}$) and $G_{\cdot OH}$ are essentially unchanged at pH = 3–11 but decreased at pH > 11 with the electron accelerator as irradiation source [42]. Thus, the explanation of the decrease in PZA degradation at alkaline condition is that $\cdot OH$ with the high reduction potential ($E^o(\cdot OH_{aq}/OH^-_{aq}) = 1.77$ V) is converted to $\cdot O^-$ with the lower reduction potential ($E^o(\cdot O^-_{aq}/OH^-_{aq}) = 1.64$ V) in the reaction (5)

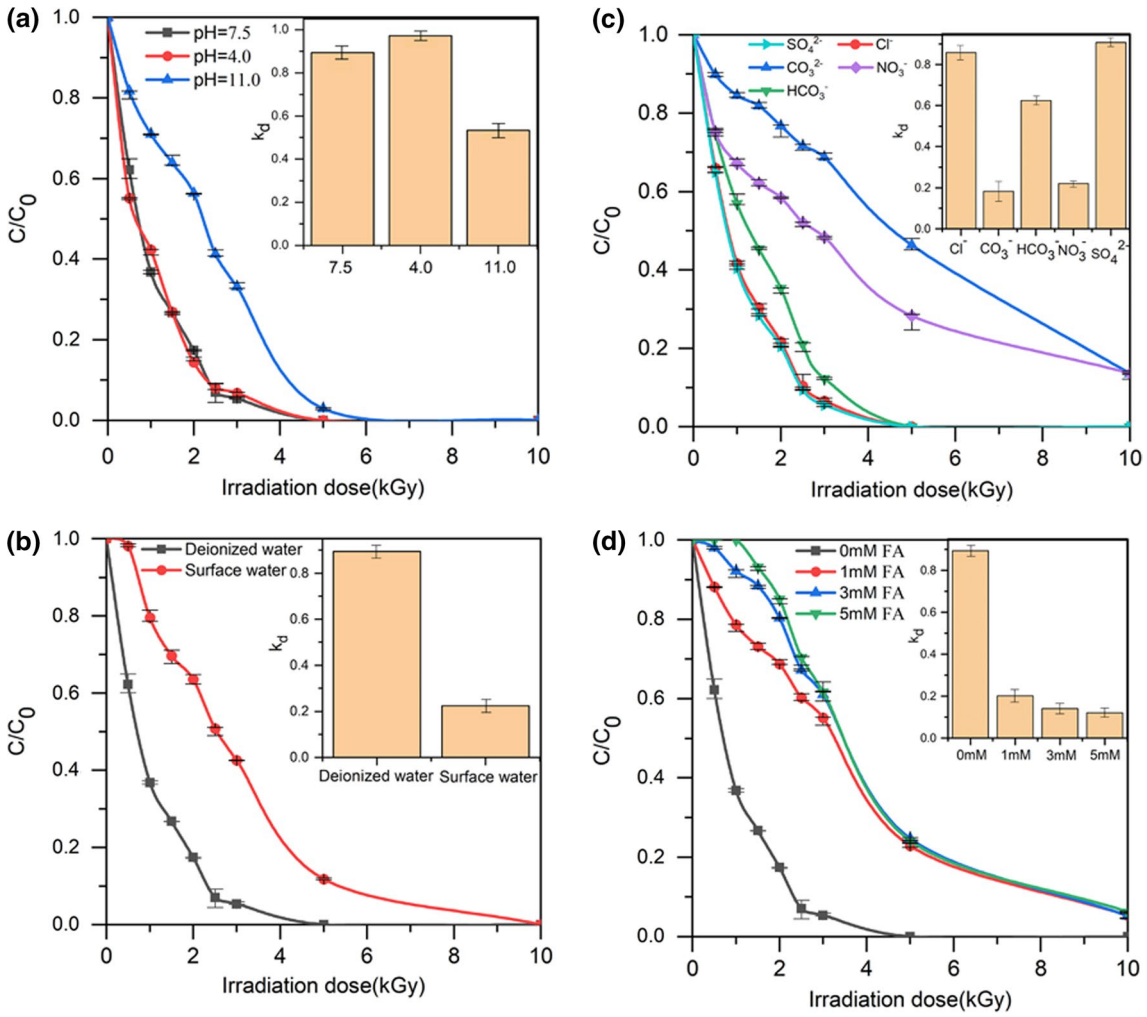

Fig. 2 **a** Degradation of PZA at different initial pH (C_0 = 0.2 mM); **b** degradation of PZA in deionized water and surface water (C_0 = 0.2 mM); **c** effects of inorganic anions (5 mM) on PZA degradation (C_0 = 0.2 mM); **d** effects of the different concentrations of fulvic acid on PZA degradation (C_0 = 0.2 mM)

[23]. In fact, ·OH is an electrophile while ·O⁻ is a nucleophile in the reactions with organic matter [23]. Due to the conjugated π-bond in the pyrazine ring, pyrazinamide is nucleophilic and reacts more readily with ·OH compared to ·O⁻. The above facts indicate that ·OH may be the main reactant in PZA degradation. Besides, the PZA degradation at pH 4 is similar to pH 7.5 because of the constant $G_{\cdot OH}$.

$$\cdot OH + OH^- \rightarrow \cdot O^- + H_2O \quad k = 1.3 \times 10^{10}\,(M\,s)^{-1} \tag{5}$$

$$e_{aq}^- + H^+ \rightarrow H\cdot \quad k = 2.3 \times 10^{10}\,(M\,s)^{-1} \tag{6}$$

The effects of different water matrices, such as deionized water and surface water on PZA degradations are shown in Fig. 2b. It indicates the vital distinction on PZA degradations in surface water in comparison to deionized water. The k_d values are 0.89 (±0.03) and 0.23 (±0.03) kGy^{-1} at deionized water and surface water, respectively. It can be explained that the ·OH generated in water radiolysis reacts with organic matter and inorganic anions in water, which leads to the decrease of ·OH concentration reacting with PZA. Thus, a higher irradiation dose is required to degrade PZA in treating surface water compared to deionized water.

Inorganic anions such as Cl^-, CO_3^{2-}, HCO_3^-, NO_3^-, and SO_4^{2-} are the common ingredients in realistic waters. As shown by Eqs. (7)–(20), the anions exhibit high chemical reactivity with the reactive species formed in water radiolysis. As shown in Fig. 2c, CO_3^{2-}, NO_3^-, and HCO_3^- inhibit the removal compared with the N_2 saturated solution. The k_d values are 0.18 (±0.05), 0.22 (±0.01), 0.63 (±0.02), 0.86 (±0.03) and 0.91 (±0.02) kGy^{-1}, in the presence of CO_3^{2-}, NO_3^-, HCO_3^-, Cl^- and SO_4^{2-}, respectively. CO_3^{2-}, NO_3^- and HCO_3^- obviously decrease the concentration of ·OH reacting with the PZA. It can be attributed that CO_3^{2-} and HCO_3^- exhibit faster reaction rates with ·OH, which lead to the reduction in the chance of the ·OH reacting with PZA. It is reported that NO_3^- can inhibit the degradation of erythromycin [21]. NO_3^- easily combines with H^+ to form HNO_3, which further reacts with ·OH [44]. However, the effect of Cl^- on the concentration of ·OH is complex due to the reactions (7) and (8). The reaction rate of forming $\cdot ClOH^-$ is $2.15 \times 10^7\ s^{-1}$, which is lower than $6.1 \times 10^9\ s^{-1}$, the reaction rate of $\cdot ClOH^-$ decomposing into Cl^- and ·OH when the concentration of Cl^- is 5 mM. Thus, the presence of Cl^- has almost no effect on the removal. SO_4^{2-} is the only anion that enhances the removal slightly, although the impact is negligible. The little impact can be explained by Eq. (13), the addition of SO_4^{2-} is converted to $\cdot SO_4^-$ which may be a stronger oxidizer for PZA compared to ·OH (Table 1).

Fulvic acid (FA) shows a potent inhibition on the degradation of PZA owing to the competition for ·OH. From Fig. 2d, at the dose of 5 kGy, the degradation percentages of PZA are 77.1%, 74.9% and 75.8% at the initial FA concentration of 1, 3 and 5 mM, respectively. It implies that PZA degradation inhibitions in different FA concentrations tend to be similar at more than 5 kGy.

Table 1 Reactions of Cl^-, CO_3^{2-}, HCO_3^-, NO_3^- and SO_4^{2-} with ·OH, ·H and e_{aq}^-

Label	Reaction	Rate constants $(M\,s)^{-1}$ or s^{-1}	References
7	$\cdot OH + Cl^- \rightarrow \cdot ClOH^-$	4.3×10^9	[43]
8	$\cdot ClOH^- \rightarrow \cdot OH + Cl^-$	6.1×10^9	[43]
9	$\cdot OH + CO_3^{2-} \rightarrow OH^- + \cdot CO_3^-$	4.0×10^8	[23]
10	$\cdot OH + HCO_3^- \rightarrow H_2O + \cdot CO_3^-$	8.5×10^6	[23]
11	$H^+ + NO_3^- \rightarrow HNO_3$	$(4.4–6.0) \times 10^8$	[44]
12	$\cdot OH + HNO_3 \rightarrow H_2O + \cdot NO_3$	$(0.88–1.2) \times 10^8$	[44, 45]
13	$\cdot OH + SO_4^{2-} \rightarrow OH^- + \cdot SO_4^-$	3.5×10^5	[23]
14	$\cdot H + Cl^- \rightarrow$ N/A	$< 1.0 \times 10^5$	[23]
15	$\cdot H + HCO_3^- \rightarrow H_2 + \cdot CO_3^-$	4.0×10^4	[23]
16	$\cdot H + NO_3^- \rightarrow OH^- + \cdot NO_2$	4.4×10^6	[23]
17	$e_{aq}^- + CO_3^{2-} \rightarrow CO_3^{3-}$	3.9×10^5	[23]
18	$e_{aq}^- + HCO_3^- \rightarrow HCO_3^{2-}$	6.0×10^5	[23]
19	$e_{aq}^- + NO_3^- \rightarrow NO_3^{2-}$	9.7×10^9	[23]
20	$e_{aq}^- + SO_4^{2-} \rightarrow$ N/A	1.0×10^6	[23]

Effects of oxidizer

As we can see from Fig. 3a, it is promoted the removal of PZA at lower H_2O_2 concentrations, such as 1 and 3 mM. However, 5 mM H_2O_2 inhibits the degradation at lower doses but promotes when the dose is more than 2.5 kGy. One possible explanation of the result is that the addition of H_2O_2 increases the ·OH concentration (Eqs. 21 and 22) [23] at lower H_2O_2 concentration. In addition, excess H_2O_2 acts as the ·OH scavenger (Eq. 23) [23] at higher H_2O_2 concentration, which leads to a decrease in the removal of PZA. It can be observed in Fig. 3b, in contrast to H_2O_2, high $K_2S_2O_8$ concentrations always promote the removal. As shown in reactions (24) and (25) [23], e_{aq}^- and H· can induce $S_2O_8^{2-}$ to product $\cdot SO_4^-$, a powerful oxidant, which increases the degradation of PZA. Moreover, $\cdot SO_4^-$ can be converted to ·OH by reactions (26) and (27) [46–48], which is beneficial for the removal.

$$e_{aq}^- + H_2O_2 \rightarrow \cdot OH + OH^- \quad k = 1.1 \times 10^{10}\,(M\,s)^{-1} \tag{21}$$

$$H\cdot + H_2O_2 \rightarrow \cdot OH + H_2O \quad k = 9.0 \times 10^7\,(M\,s)^{-1} \tag{22}$$

$$\cdot OH + H_2O_2 \rightarrow HO_2\cdot + H_2O \quad k = 2.7 \times 10^7\,(M\,s)^{-1} \tag{23}$$

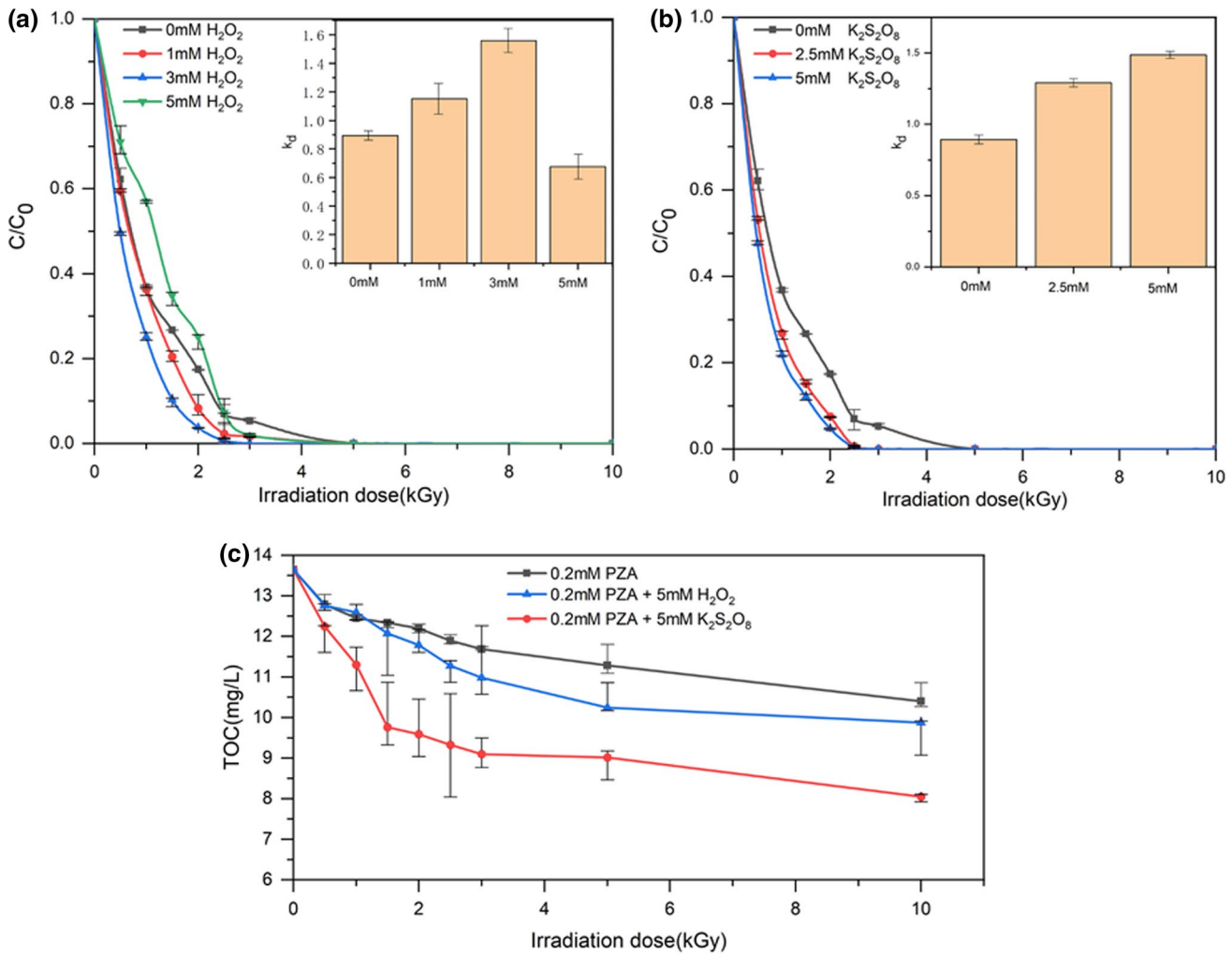

Fig. 3 **a** Effects of the different concentrations of H_2O_2 on PZA degradation ($C_0 = 0.2$ mM); **b** effects of the different concentrations of $K_2S_2O_8$ on PZA degradation ($C_0 = 0.2$ mM); **c** effects of H_2O_2 and $K_2S_2O_8$ on the PZA mineralization ($C_0 = 0.2$ mM)

$$e_{aq}^- + S_2O_8^{2-} \rightarrow {}^{\cdot}SO_4^- + SO_4^{2-} \quad k = 1.1 \times 10^{10}\,(M\,s)^{-1} \tag{24}$$

$$H^{\cdot} + S_2O_8^{2-} \rightarrow {}^{\cdot}SO_4^- + SO_4^{2-} + H^+ \quad k = 2.5 \times 10^{7}\,(M\,s)^{-1} \tag{25}$$

$${}^{\cdot}SO_4^- + H_2O \rightarrow {}^{\cdot}OH + SO_4^{2-} \quad k = 3.6 \times 10^{2}\,s^{-1} \tag{26}$$

$${}^{\cdot}SO_4^- + OH^- \rightarrow {}^{\cdot}OH + SO_4^{2-} \quad k = 1.4 \times 10^{7}\,(M\,s)^{-1} \tag{27}$$

TOC is regarded as a reliable indicator to estimate the level of organic pollution in water [49]. Figure 3c indicates that the addition of H_2O_2 and $K_2S_2O_8$ enhance the mineralization of PZA at high doses. The effect of H_2O_2 on the PZA mineralization is complex. In the presence of 5 mM H_2O_2, there is the slight inhibition at the lower doses but a little promotion at the higher doses, and the TOC value can be decreased from 13.65 to 9.88 mg L^{-1} at 10 kGy. However, the addition of $K_2S_2O_8$ always promotes the PZA mineralization, and decreases the TOC from 13.65 to 8.05 mg L^{-1} at 10 kGy, proving that $K_2S_2O_8$ is more potential to decrease TOC.

Effects of scavengers

In Fig. 4, we compare the effects of radicals' scavengers such as N_2O and tert-butanol (t-BuOH) on PZA degradations. The addition of N_2O gas significantly contributes to the degradation of PZA compared to the N_2. Thus, it is reasonable to suppose that ${}^{\cdot}OH$ is the primary reactant in PZA degradation for N_2O is beneficial for increasing the concentration of ${}^{\cdot}OH$ by Eq. (28) [23]. Moreover, t-BuOH is a typical ${}^{\cdot}OH$ scavenger by Eq. (29) [23], and the addition of it reduces the efficiency of PZA removal. It also confirms that ${}^{\cdot}OH$ is

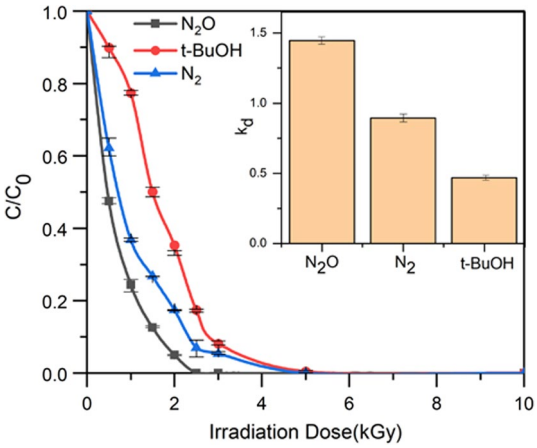

Fig. 4 Degradation of PZA at different scavengers (C_0 = 0.2 mM)

a more dominant reactive species in all possible reactants generated by water radiolysis from the opposite perspective.

$$e_{aq}^{-} + N_2O + H_2O \rightarrow {}^{\cdot}OH + N_2 + OH^{-} \quad k = 9.1 \times 10^{9}\ (M\ s)^{-1} \tag{28}$$

$${}^{\cdot}OH + t - BuOH \rightarrow {}^{\cdot}CH_2C\left(CH_3\right)_2OH + H_2O \quad k = 6.0 \times 10^{8}\ (M\ s)^{-1} \tag{29}$$

Analysis of degradation mechanism and quantum chemistry calculation

Table S2 (Supplementary Material) shows the detected compounds according to the data of the LC-QTOF-MS analysis and the IC analysis. The results of the IC analysis show decreased formic acid concentrations and increased ammonium cation concentration following the increasing irradiation dose. It can be attributed to the mineralization of formic acid in the presence of ·OH and that ammonium cation is hard to oxidize to nitrate. Compared to the experiment of Fenton, 5-hydroxypyrazinamide and NH_3 are detected in this experiment, but pyrazin-2-ylmethanol, pyrazine, acetamide, and acetic acid are not found. It shows that detailed degradation mechanism of PZA using EBI is different from Fenton [18].

From Scheme 1 and Table S4, the first reaction is free radicals attacking the aromatic ring or amide group. Four intermediates, IM1, IM2, IM3 and IM4, are formed via the reaction between ·OH and the C of the aromatic ring, while IM5 is hardly formed due to both a higher free energy barrier (21.73 kcal mol^{-1}) and an unfavorable reaction free energy change (+ 15.24 kcal mol^{-1}). A lower reaction rate constant (1.01×10^{-3} $(M\ s)^{-1}$) also indicates that the generation of IM5 is impractical. In all reactions between PZA and ·OH, the preferred reaction pathway is the reaction (1–2a) owing to the lowest free energy (9.05 kcal mol^{-1}). IM2 continuously reacts with ·OH to form water and IM9, which isomerized to IM10 in water. The free energy barrier for the isomerization with water (11.01 kcal mol^{-1}) is lower than without water (35.96 kcal mol^{-1}), and the reaction rate of the former (7.26×10^{4} s^{-1}) is also higher than the latter (2.91×10^{-5} s^{-1}), so water plays the catalytic role in the isomerization. Due to the lower free energy barrier, IM10 can be converted via the TS1-2d to IM11, which further reacts with ·OH to form IM8 (2-Hydroxypyrazine) detected by QTOF and IM6. Another possible pathway to form IM8 is the pathways (1–1b and 1–1c), the radical reaction between IM1 and ·OH can generate carbamic acid and IM7 converted further to IM8. IM3 and IM4, as the active intermediates, react rapidly with ·OH via the reaction pathways (1–3b and 1–4b) to form ultimately IM12 found by QTOF.

In addition, H· as reductive species may attack PZA through the reaction pathways (2–1a)–(2–6a) whose free energy barriers are 10.42, 8.53, 9.91, 9.92, 8.36 and 8.92 kcal mol^{-1}, respectively. Pathway (2–7a) and (2–8a) are hardly achieved due to the higher free energy barriers of 15.57 and 15.07 kcal mol^{-1} and the lower reaction rate constants of 7.24×10^{1} $(M\ s)^{-1}$ and 1.50×10^{4} $(M\ s)^{-1}$. There is another pathway to generate IM15, hydrogen ions combined with the charged complex (IM22) formed by electron transfer of PZA and hydrated electrons. The instability of the radical intermediates generated by pathways (2–1a)–(2–6a) decides that they are highly susceptible to ·OH or H·. The calculations show that these intermediates tend to react with ·OH to form PZA and water. Moreover, the leaving of the amide group is hardly occurred due to the endergonic process by 4.13 kcal mol^{-1} and the lower reaction rate constant (1.21×10^{1} s^{-1}). Therefore, it cannot produce pyrazine in treating PZA solution by EBI.

Based on the analysis of degradation products and quantum chemical simulations, a possible degradation pathway is shown in Scheme 2. IM8 and IM 12 are the primary stable intermediate. IM12 is converted to IM23 under further attack of ·OH, which IM23 can undergo the break of C–C bond via transition state TS4b to generate IM24 and ·$CONH_2$. Similar to the isomerization of IM7, IM24 can also be isomerized to IM26. Likewise, 2-Hydroxypyrazine can be further oxidized via the reactions (5a–5b) to form IM26. IM26 undergoes the break of the six-membered ring by ·OH to produce IM28. The calculations show that the hydrogen ionization reaction in the carboxyl group of IM28 is less favorable due to the endergonic process and the decrease in pH in the radiolytic degradation of the organic molecule. In fact, the occurrence of the reaction (5e) is more thermodynamically favorable. In the presence of H·, the C-N single bond of IM29 breaks to form IM30 found by QTOF and IM6. The addition reaction is then carried out in the C-N double bond of IM30, thus forms to IM32, which is further oxidized to IM34 through

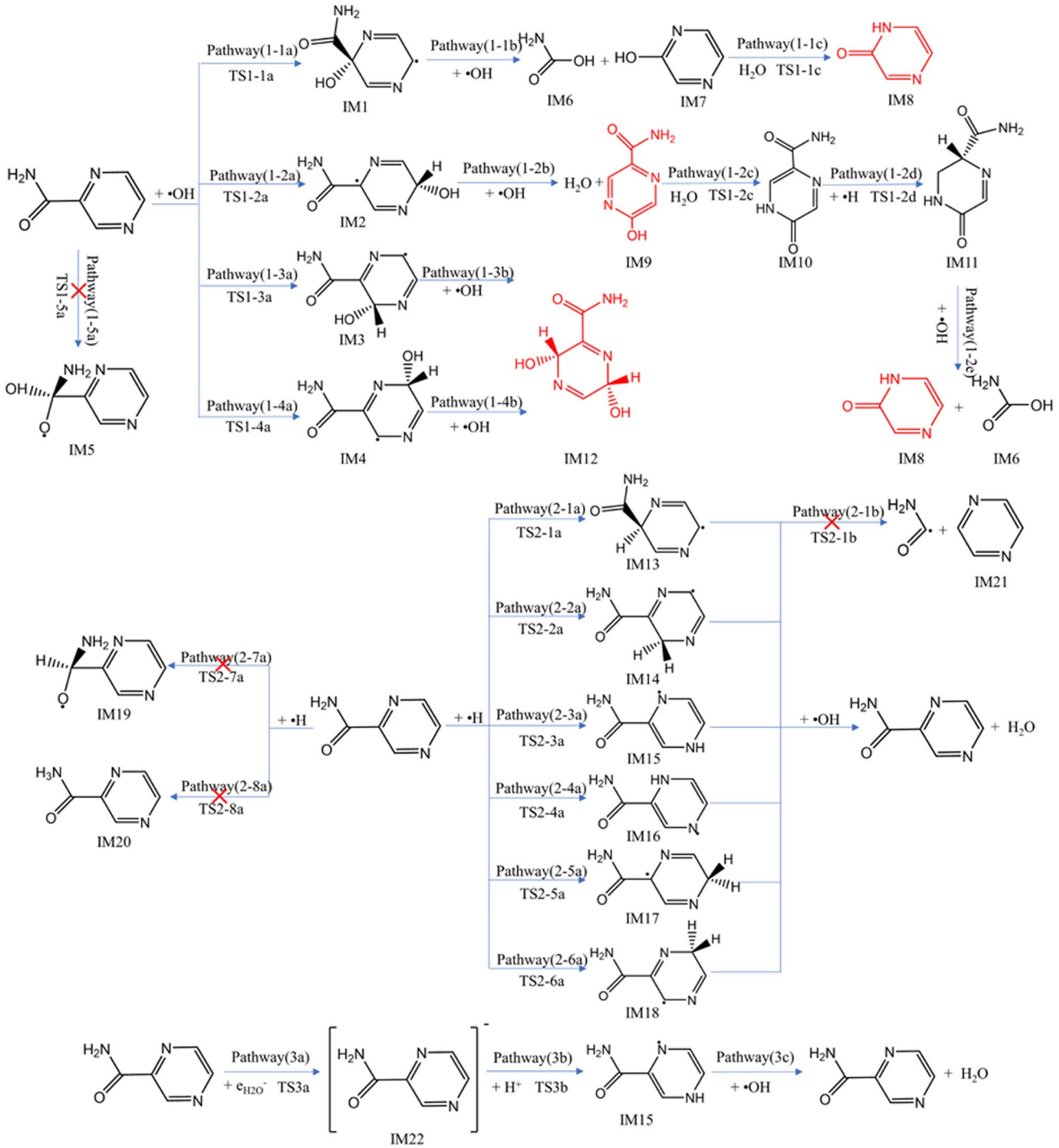

Scheme 1 Proposed the degradation processes of PZA by EBI

the reactions (5i and 5j). IM34 can be decomposed to IM35, ·CHO and water with the action of ·OH due to the instability of two hydroxyl groups on the same carbon atom. ·OH is combined with ·CHO to produce formic acid in the experiment, and IM35 to produce water and IM37. The calculations of IM37 show that the hydrogen ionization reaction in the carboxyl group and the reaction between IM37 and ·OH are hard to carry out due to the endergonic process. The analysis of QTOF proves the abundant presence of IM37. It is found that IM37 tends to react with hydrated electrons in electron exchange. The free energy barrier of this reaction is 7.53 kcal mol^{-1}, which is lower than ·OH or H·. Further, the

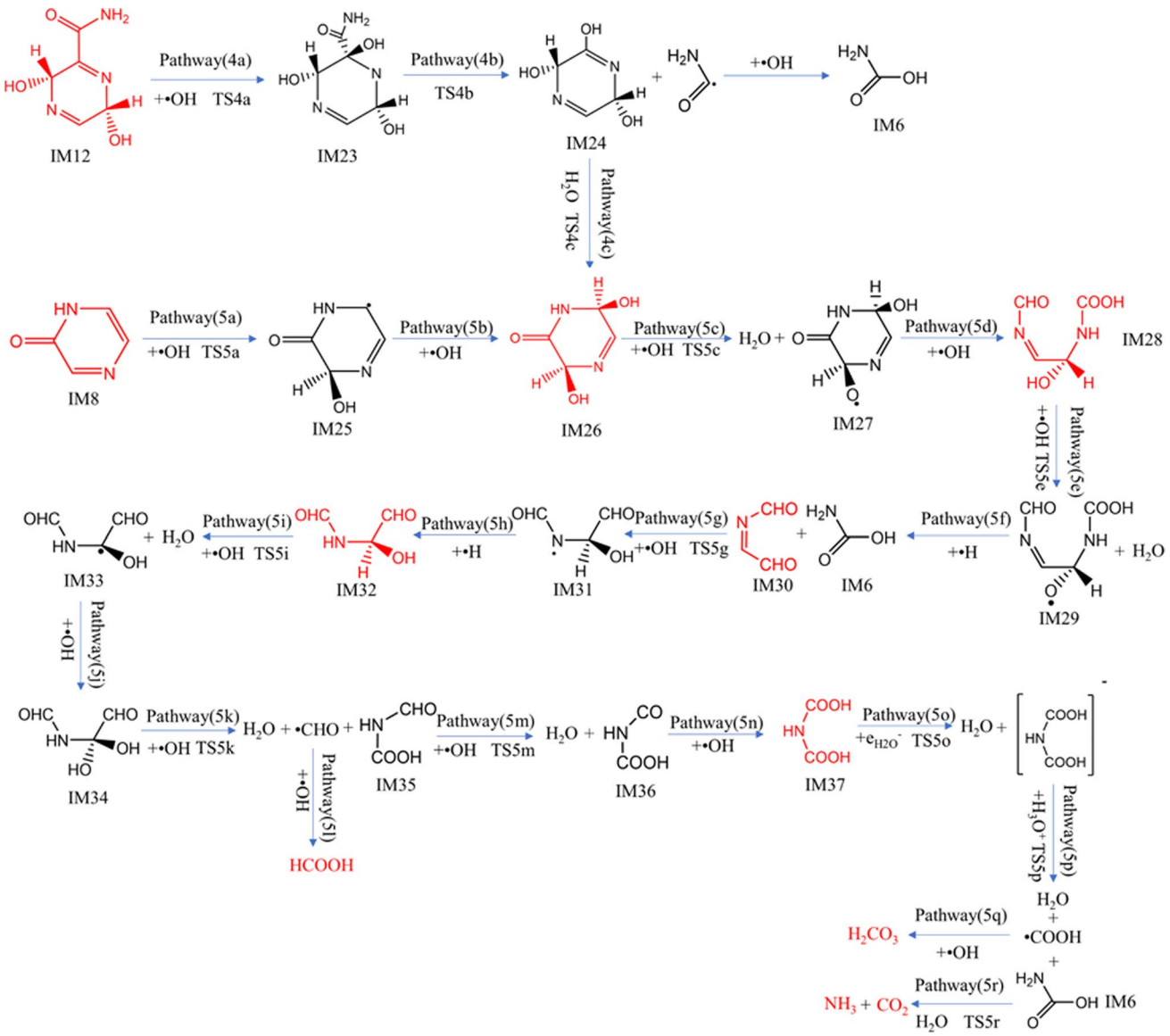

Scheme 2 Proposed the possible degradation processes of the main intermediates by EBI

generated charged complex reacts rapidly with the hydrated proton to finally form the carboxyl group and NH_2COOH. The carboxyl group can combine with ·OH to produce carbonic acid. It is reported that NH_2COOH can be decomposed to NH_3 and CO_2 in aqueous [50]. The calculation of NH_2COOH also shows that it can undergo the hydrogen transfer reaction to produce NH_3 and CO_2.

Conclusions

The present work showed that EBI was efficient to degrade PZA. The results showed that electron beam irradiation was highly effective in the removal of PZA from water. Some inorganic anions and fulvic acid exhibited inhibition of the PZA degradation in this study. The inhibition effects of inorganic anions were $CO_3^{2-} > NO_3^- > HCO_3^-$ while Cl^- and SO_4^{2-} have negligible effects on the degradation of PZA. $K_2S_2O_8$ and lower concentrations of H_2O_2, such as 1 and 3 mM, could effectively promote the removal of PZA. However, 5 mM H_2O_2 inhibited the degradation at lower doses, and promoted the degradation at higher doses. In addition, TOC removal efficiency increased from 23.8% to 41.0% and 27.6% with the additions of 5 mM $K_2S_2O_8$ and H_2O_2, respectively. Thus, $K_2S_2O_8$ was the better additive to enhance the mineralization of PZA. The experiments of radical scavengers showed that ·OH was the main reactive species in PZA degradation. Moreover, the degradation mechanism of PZA

by EBI was suggested by combining LCMS, IC and quantum chemiscal calculations. It was confirmed that both $^{\cdot}OH$ and $H^{\cdot}$ played a significant role in the degradation of intermediates and the mineralization of PZA.

Supplementary Information The online version contains supplementary material available at https://doi.org/10.1007/s10967-021-07757-1.

Acknowledgements We strongly appreciate the High Performance Computing Center of Shanghai University, and Shanghai Engineering Research Center of Intelligent Computing System (No. 19DZ2252600) and the Deepcomp7000 and ScGrid of Supercomputing Center and Computer Network Information Center of Chinese Academy of Sciences for providing the computing resources and technical support.

Funding This work was financially supported by the National Natural Science Foundation of China (Nos. 11975147, 11875185, 41773121, 11775138) and National Key Research and Development Project (No. 2020YFC1808200).

Declarations

Conflict of interest The authors declare that they have no conflict of interest.

References

1. Zhang QQ, Ying GG, Pan CG, Liu YS, Zhao JL (2015) Comprehensive evaluation of antibiotics emission and fate in the river Basins of China: source analysis, multimedia modeling, and linkage to bacterial resistance. Environ Sci Technol 49(11):6772–6782
2. Sarmah AK, Meyer MT, Boxall ABA (2006) A global perspective on the use, sales, exposure pathways, occurrence, fate and effects of veterinary antibiotics (VAs) in the environment. Chemosphere 65(5):725–759
3. Michael I, Rizzo L, McArdell CS, Manaia CM, Merlin C, Schwartz T, Dagot C, Fatta-Kassinos D (2013) Urban wastewater treatment plants as hotspots for the release of antibiotics in the environment: a review. Water Res 47(3):957–995
4. Watkinson AJ, Murby EJ, Costanzo SD (2007) Removal of antibiotics in conventional and advanced wastewater treatment: Implications for environmental discharge and wastewater recycling. Water Res 41(18):4164–4176
5. Danner MC, Robertson A, Behrends V, Reiss J (2019) Antibiotic pollution in surface fresh waters: occurrence and effects. Sci Total Environ 664:793–804
6. Organization WH (2019) Global tuberculosis report 2019. World Health Organization
7. Donald PR, McIlleron H (2009) Chapter 59—antituberculosis drugs. In: Schaaf HS, Zumla AI, Grange JM et al (eds) Tuberculosis. W.B. Saunders, Edinburgh, pp 608–617
8. Kori R, Saxena A, Mokhle S, Goutam V, Kulshreshtha A, Ramnani V, Parmar M (2019) Bioassay study on treated effluent of basic drug industries of Mandideep industrial area of Madhya Pradesh. India Biodivy Int J 3(5):202–207
9. Chen YS, Xi XP, Yu G, Cao QM, Wang B, Vince F, Hong YW (2015) Pharmaceutical compounds in aquatic environment in China: locally screening and environmental risk assessment. Front Env Sci Eng 9(3):394–401
10. Njire M, Tan YJ, Mugweru J, Wang CW, Guo JT, Yew WW, Tan SY, Zhang TY (2016) Pyrazinamide resistance in Mycobacterium tuberculosis: review and update. Adv Med Sci Poland 61(1):63–71
11. Zignol M, Dean AS, Alikhanova N, Andres S, Cabibbe AM, Cirillo DM, Dadu A, Dreyer A, Driesen M, Gilpin C, Hasan R, Hasan Z, Hoffner S, Husain A, Hussain A, Ismail N, Kamal M, Mansjo M, Mvusi L, Niemann S, Omar SV, Qadeer E, Rigouts L, Ruesch-Gerdes S, Schito M, Seyfaddinova M, Skrahina A, Tahseen S, Wells WA, Mukadi YD, Kimerling M, Floyd K, Weyer K, Raviglione MC (2016) Population-based resistance of Mycobacterium tuberculosis isolates to pyrazinamide and fluoroquinolones: results from a multicountry surveillance project. Lancet Infect Dis 16(10):1185–1192
12. Huber MM, Canonica S, Park GY, Von Gunten U (2003) Oxidation of pharmaceuticals during ozonation and advanced oxidation processes. Environ Sci Technol 37(5):1016–1024
13. Klavarioti M, Mantzavinos D, Kassinos D (2009) Removal of residual pharmaceuticals from aqueous systems by advanced oxidation processes. Environ Int 35(2):402–417
14. Khan A, Mir NA, Haque MM, Muneer M (2013) Photocatalysed mineralization of three selected antibacterial drugs, kanamycin acid sulfate, ampicillin and pyrazinamide in aqueous suspensions of TiO_2/H_2O_2. Mater Focus 2(5):335–341
15. Vargas F, Rivas C, Diaz Y, Fuentes A (2003) Photodegradation pathways and the in vitro phototoxicity of pyrazinamide, a phototoxic antitubercular drug. J Photoch Photobio B 72(1–3):87–94
16. Cantwell RE, Hofmann R (2011) Ultraviolet absorption properties of suspended particulate matter in untreated surface waters. Water Res 45(3):1322–1328
17. Conde-Morales II, Hinojosa-Reyes L, Guzman-Mar JL, Hernandez-Ramirez A, Saenz-Tavera ID, Villanueva-Rodriguez M (2020) Different iron oxalate sources as catalysts on pyrazinamide degradation by the photo-Fenton process at different pH values. Water Air Soil Poll 231(8):1–15
18. Arhoutane MR, Yahya MS, El Karbane M, Guessous A, Chakchak H, El Kacemi K (2019) Removal of pyrazinamide and its by-products from water: treatment by electro-Fenton process and feasibility of a biological post-treatment. Medit J Chem 8(1):53–65
19. Wang JL, Zhuan R (2020) Degradation of antibiotics by advanced oxidation processes: an overview. Sci Total Environ. https://doi.org/10.1016/j.scitotenv.2019.135023
20. Guin JP, Bhardwaj YK, Varshney L (2017) Efficient degradation of butylparaben by gamma radiolysis. Appl Radiat Isotopes 122:21–27
21. Chu LB, Zhuan R, Chen D, Wang JL, Shen YP (2019) Degradation of macrolide antibiotic erythromycin and reduction of antimicrobial activity using persulfate activated by gamma radiation in different water matrices. Chem Eng J 361:156–166
22. Paul J, Rawat KP, Sarma KSS, Sabharwal S (2011) Decoloration and degradation of Reactive Red-120 dye by electron beam irradiation in aqueous solution. Appl Radiat Isotopes 69(7):982–987
23. Buxton GV, Greenstock CL, Helman WP, Ross AB (1988) Critical review of rate constants for reactions of hydrated electrons, hydrogen atoms and hydroxyl radicals ($^{\cdot}OH/O^{-}$) in Aqueous solution. J Phys Chem Ref Data 17(2):513–886
24. Xu G, Yao JZ, Tang L, Yang XY, Zheng M, Wang H, Wu MH (2015) Electron beam induced degradation of atrazine in aqueous solution. Chem Eng J 275:374–380
25. Jeong J, Song WH, Cooper WJ, Jung J, Greaves J (2010) Degradation of tetracycline antibiotics: mechanisms and kinetic studies for advanced oxidation/reduction processes. Chemosphere 78(5):533–540
26. Pelalak R, Alizadeh R, Ghareshabani E, Heidari Z (2020) Degradation of sulfonamide antibiotics using ozone-based advanced oxidation process: experimental, modeling, transformation

mechanism and DFT study. Sci Total Environ. https://doi.org/10.1016/j.scitotenv.2020.139446
27. Lyu GX, Shi GS, Tang L, Fang HP, Wu MH (2017) Mechanism of degradation of a nitrogenous heterocycle induced by a reductive radical: decomposition of a sym-triazine ring. Phys Chem Chem Phys 19(14):9354–9357
28. Dou MM, Wang J, Gao BR, Xu C, Yang F (2020) Photocatalytic difference of amoxicillin and cefotaxime under visible light by mesoporous g-C3N4: mechanism, degradation pathway and DFT calculation. Chem Eng J. https://doi.org/10.1016/j.cej.2019.123134
29. Yu H, Ge P, Chen JW, Xie HB, Luo Y (2017) The degradation mechanism of sulfamethoxazole under ozonation: a DFT study. Environ Sci-Proc Imp 19(3):379–387
30. Ho JM, Klamt A, Coote ML (2010) Comment on the correct use of continuum solvent models. J Phys Chem A 114(51):13442–13444
31. Marenich AV, Cramer CJ, Truhlar DG (2009) Universal solvation model based on solute electron density and on a continuum model of the solvent defined by the bulk dielectric constant and atomic surface tensions. J Phys Chem B 113(18):6378–6396
32. Frisch MJ, Trucks GW, Schlegel HB, Scuseria GE, Robb MA, Cheeseman JR, Scalmani G, Barone V, Petersson GA, Nakatsuji H, Li X, Caricato M, Marenich AV, Bloino J, Janesko BG, Gomperts R, Mennucci B, Hratchian HP, Ortiz JV, Izmaylov AF, Sonnenberg JL, Williams, Ding F, Lipparini F, Egidi F, Goings J, Peng B, Petrone A, Henderson T, Ranasinghe D, Zakrzewski VG, Gao J, Rega N, Zheng G, Liang W, Hada M, Ehara M, Toyota K, Fukuda R, Hasegawa J, Ishida M, Nakajima T, Honda Y, Kitao O, Nakai H, Vreven T, Throssell K, Montgomery Jr. JA, Peralta JE, Ogliaro F, Bearpark MJ, Heyd JJ, Brothers EN, Kudin KN, Staroverov VN, Keith TA, Kobayashi R, Normand J, Raghavachari K, Rendell AP, Burant JC, Iyengar SS, Tomasi J, Cossi M, Millam JM, Klene M, Adamo C, Cammi R, Ochterski JW, Martin RL, Morokuma K, Farkas O, Foresman JB, Fox DJ (2009) Gaussian 09 Rev. D.01, Wallingford, CT
33. Zhao Y, Truhlar DG (2008) The M06 suite of density functionals for main group thermochemistry, thermochemical kinetics, noncovalent interactions, excited states, and transition elements: two new functionals and systematic testing of four M06-class functionals and 12 other functionals. Theor Chem Acc 120(1–3):215–241
34. Goerigk L, Hansen A, Bauer C, Ehrlich S, Najibi A, Grimme S (2017) A look at the density functional theory zoo with the advanced GMTKN55 database for general main group thermochemistry, kinetics and noncovalent interactions. Phys Chem Chem Phys 19(48):32184–32215
35. Goerigk L, Grimme S (2011) A thorough benchmark of density functional methods for general main group thermochemistry, kinetics, and noncovalent interactions. Phys Chem Chem Phys 13(14):6670–6688
36. Lu T, Chen Q (2021) Shermo: a general code for calculating molecular thermochemistry properties. Comput Theor Chem 1200:113249. https://doi.org/10.1016/j.comptc.2021.113249
37. Kanchanakungwankul S, Zheng J, Alecu IM, Lynch BJ, Zhao Y, Truhlar DG (2020) Database of frequency scale factors for electronic model chemistried. http://comp.chem.umn.edu/freqscale/190107_Database_of_Freq_Scale_Factors_v4.pdf
38. Neese F (2012) The ORCA program system. WIREs Computational Molecular Science 2(1):73–78
39. Neese F (2018) Software update: the ORCA program system, version 4.0. WIREs Comput Mol Sci 8(1):e1327
40. Truhlar DG, Garrett BC, Klippenstein SJ (1996) Current status of transition-state theory. J Phys Chem Us 100(31):12771–12800
41. Skodje RT, Truhlar DG (1981) Parabolic tunneling calculations. J Phys Chem Us 85(6):624–628
42. Ferradini C, Jay-Gerin JP (2000) The effect of pH on water radiolysis: a still open question—a minireview. Res Chem Intermediat 26(6):549–565
43. Atinault E, De Waele V, Schmidhammer U, Fattahi M, Mostafavi M (2008) Scavenging of es− and OH radicals in concentrated HCl and NaCl aqueous solutions. Chem Phys Lett 460(4):461–465
44. Wang JL, Zhuan R, Chu LB (2019) The occurrence, distribution and degradation of antibiotics by ionizing radiation: an overview. Sci Total Environ 646:1385–1397
45. Poskrebyshev GA, Neta P, Huie RE (2001) Equilibrium constant of the reaction ·OH + HNO3 ⇆ H2O + NO_3 in aqueous solution. J Geophys Res Atmos 106(5):4995–5004
46. Tang Y, Thorn RP, Mauldin RL, Wine PH (1988) Kinetics and spectroscopy of the SO4− radical in aqueous solution. J Photochem Photobiol A 44(3):243–258
47. McElroy WJ, Waygood SJ (1990) Kinetics of the reactions of the SO_4^- radical with SO_4^-. $S_2O_{82}^-$. H_2O and Fe^{2+}. In: Restelli G, Angeletti G (eds) Physico-chemical behaviour of atmospheric pollutants: air pollution research reports. Springer, Dordrecht, pp 251–256
48. Bao ZC, Barker JR (1996) Temperature and ionic strength effects on some reactions involving sulfate radical [SO_4-(aq)]. J Phys Chem-Us 100(23):9780–9787
49. Shi YM, Xu LF, Gong DQ, Lu J (2010) Effects of sterilization treatments on the analysis of TOC in water samples. J Environ Sci China 22(5):789–795
50. Chen YJ, Nuevo M, Hsieh JM, Yih TS, Sun WH, Ip WH, Fung HS, Chiang SY, Lee YY, Chen JM, Wu CYR (2007) Carbamic acid produced by the UV/EUV irradiation of interstellar ice analogs. Astron Astrophys 464(1):253–257